First-principles study of metal–graphene interfaces

Cheng Gong,[1] Geunsik Lee,[1] Bin Shan,[1,4] Eric M. Vogel,[1,2] Robert M. Wallace,[1,2] and Kyeongjae Cho[1,3,a)]

[1]*Department of Materials Science and Engineering, The University of Texas at Dallas, Richardson, Texas 75080, USA*
[2]*Department of Electrical Engineering, The University of Texas at Dallas, Richardson, Texas 75080, USA*
[3]*Department of Physics, The University of Texas at Dallas, Richardson, Texas 75080, USA*
[4]*Department of Materials Science and Engineering, Huazhong University of Science and Technology, Wuhan 430073, China*

(Received 23 June 2010; accepted 30 October 2010; published online 28 December 2010)

Metal-graphene contact is a key interface in graphene-based device applications, and it is known that two types of interfaces are formed between metal and graphene. In this paper, we apply first-principles calculations to twelve metal-graphene interfaces and investigate the detailed interface atomic and electronic structures of physisorption and chemisorption interfaces. For physisorption interfaces (Ag, Al, Cu, Cd, Ir, Pt, and Au), Fermi level pinning and Pauli-exclusion-induced energy-level shifts are shown to be two primary factors determining graphene's doping types and densities. For chemisorption interfaces (Ni, Co, Ru, Pd, and Ti), the combination of Pauli-exclusion-induced energy-level shifts and hybridized states' repulsive interactions lead to a band gap opening with metallic gap states. For practical applications, we show that external electric field can be used to modulate graphene's energy-levels and the corresponding control of doping or energy range of hybridization. © *2010 American Institute of Physics*.
[doi:10.1063/1.3524232]

I. INTRODUCTION

Since the experimental realization of a single layer graphene,[1,2] which is a strictly two dimensional network of hexagonally arranged carbon atoms, an increasing amount of research has been devoted to the study of its physical properties and practical applications.[3–9] As a two-dimensional (2D) sheet with monoatomic thickness, graphene's properties are shown to be very sensitive to the surrounding environment.[10–24] Much research effort has been devoted to the study of interaction between graphene and silicon carbide,[10,11] silicon dioxide,[12] metal surfaces,[13–24] and other dielectric surfaces. These graphene–substrate interactions are of practical significance during the process of graphene synthesis and graphene-based device fabrication. In particular, metal-graphene interfaces are formed and used in material production,[14,25] electrical measurement,[19] and device fabrication[5,26] where metals play different roles as substrate catalysts, probes and source/drain electrodes, respectively. Due to the minuscule nature of the device material (e.g., single layer graphene), the interface may have substantial influence on the device performance in all these cases.

In an experimental measurement,[19] metal electrodes are shown to dope the graphene at the metal–graphene (M–G) interfaces and induce asymmetric conductance-V_{gate} curves. *Ab initio* study of metal-graphene interfaces has shown that graphene is doped by metal electrode.[18] Recent experimental studies of metal–graphene interfaces have shown that different metals show different interfacial bonding (strong for Ni and Ti/Au and weak for Pt and Au) and that carbide bonds are formed at Ti–G but not at Pt–G interfaces.[27] The metal substrate and graphene can form either a physisorption interface with charge transfer,[18,23,24,28] or a chemisorption interface with orbital hybridization.[13–15,17,22,28,30–32] A physisorption interface does not form chemical bonding and preserves graphene's intrinsic π-band structure, but a chemisorption interface forms metal carbide bonding and disturbs graphene's electronic structure through a strong hybridization of metal's *d*-orbital and graphene's π-orbital. At physisorption interfaces, recent theoretical[18] and experimental[20] studies have shown that graphene can be doped by metal contact, and specifically Cu with a work function up to ~5.2 eV can *n*-type dope graphene, which has an intrinsic work function (WF) ~4.6 eV. Such doping behavior cannot be explained by the conventional Schottky–Mott model, and Giovannetti *et al.*[18] have developed a phenomenological model in which chemical interaction (Pauli's repulsive interaction) and electron transfer are assigned as two main factors for interfacial doping. Even though this model analysis has identified the key concepts and explained the doping behavior, a further study is needed to gain deeper understanding on the nature of the interface interaction and the origin of interface dipole.

Furthermore, chemisorption interfaces, compared to physisorption interfaces, are more likely to form realistic electrode contacts because of their stronger bonding to graphene. It is worthwhile to note that recently Vanin *et al.* have applied van der Waals (vdW) density functional theory[29] to study metal–graphene interfaces and obtained the results of all weakly bonded interfaces which are different from previous density functional theory calculations. However, their finding (that all metals form weak bonding to graphene) does not agree with experimental observations

a)Electronic mail: kjcho@utdallas.edu.

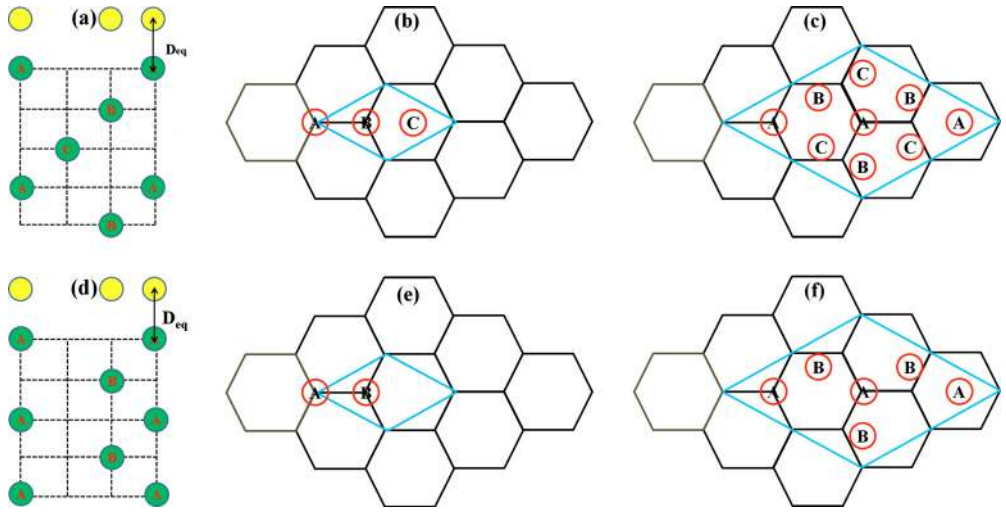

FIG. 1. (Color online) Atomic model of vertical stacking of graphene adsorbed on (a) (111) surfaces of face-centered cubic (FCC) metals and (d) (0001) surfaces of hexagonal close-packed (HCP) metals. Graphene adsorbed on (b) 1×1 unit cell of Ni and Cu FCC (111) surfaces, (c) 2×2 unit cell of Ag, Al, Ir, Pt, Au, and Pd FCC (111) surfaces, (e) 1×1 unit cell of Co HCP (0001) surface, and (f) 2×2 unit cell of Cd, Ru, and Ti HCP (0001) surfaces.

based on angle-resolved photoemission spectroscopy (ARPES) (Refs. 30 and 31) and low-energy electron diffraction (LEED) (Ref. 32) measurements, and consequently vdW DFT is not more accurate than conventional DFT methods for the metal-graphene interface modeling study.[33] Thus, a DFT modeling study on chemisorption interfaces has more practical relevance to experimental studies. At chemisorption interfaces, the electronic structure is much more complicated because of the chemical interaction between metal *d*-states and graphene π-states. However, detailed atomic scale investigations based on *ab initio* studies are currently lacking, and the physical and electronic behaviors of these interfaces are not yet well understood. In this work, we use *ab initio* methods to gain a fundamental understanding of the electronic properties at both physisorption and chemisorption interfaces. For the physisorption interfaces, the Pauli-exclusion interaction (between carbon π-orbitals and metal *s*-orbitals) plays the primary role in shifting the surface chemical potentials of metal and graphene leading to interface charge transfer. For the chemisorption interfaces, the chemical interaction of carbon π-orbitals and metal *d*-orbitals induces a gap opening in graphene π-band structure. Application of external electric field (EEF) is shown to change the relative alignment of the M–G interface electronic structures leading to possible mechanisms of graphene electrode contact control. In order to focus on the main physical mechanism of the M–G interface interaction, in this paper, we have not included topological ripples[15,16] of graphene caused by lattice mismatch between metal and graphene into considerations.

II. METHODOLOGY

To investigate the atomic and electronic structures of the metal-graphene interfaces, we use Vienna *Ab initio* simulation package (VASP) (Ref. 34) with the projected augmented wave (PAW) (Ref. 35) pseudopotentials with local density approximation. Energy cutoff of 400 eV is chosen for the plane-wave basis which shows a good convergence in total energy and Hellmann–Feynman forces. Graphene's lattice size is fixed at the optimized value 2.46 Å, and 12 metal surfaces' lattice sizes are strained to fit onto graphene's 1×1 or 2×2 unit cell. When adjusting metal's lattice size onto the fixed graphene's lattice, all metals' lattice mismatches are smaller than 5% (as shown in Fig. 1 and Table I) compared with the experimental values.[36] In all supercells of the 12 metal–graphene interface models studied here, at least 18 Å vacuum regions in the z-direction are included to minimize the interaction between adjacent image cells as well as to accommodate an effective EEF in the vacuum region.[37] Five metal atomic layers are adopted to represent the metal electrode, and this model has been tested to show that the slab is thick enough to accurately model the interface properties at metal-graphene contact.[28] During atomic structure relaxation calculations to find the most energetically favorable structures, all the metal atoms are fully relaxed with the

TABLE I. Calculated equilibrium interfacial distances (Deq), binding energies of complexes (Eb), WFs of clean metals (WF), Fermi level shifts relative to the Dirac point (ΔE_F), charge transferred to graphene (Δq), and lattice strain of metals are listed. Positive (negative) lattice mismatch represents expansion (compression) of metal lattice. The first seven metals form physisorption interfaces, and the last five metals form chemisorptions interfaces with graphene. Graphene's intrinsic WF in our calculation is 4.77 eV.

	Deq (Å)	Eb (eV/C atom)	WF (eV)	ΔE_F (eV)	Lattice mismatch (%)
Ag	3.26	−0.031	4.96	0.35	−1.8
Al	3.59	−0.042	4.28	0.49	−0.8
Cu	2.96	−0.030	5.35	0.47	−3.6
Cd	3.64	−0.028	4.21	0.44	−4.7
Ir	3.44	−0.033	5.82	−0.23	4.6
Pt	3.18	−0.046	5.98	−0.31	2.5
Au	3.27	−0.037	5.55	−0.20	−1.6
Ni	2.07	−0.133	5.47	⋯	−1.2
Co	2.11	−0.432	5.32	⋯	−2.0
Ru	2.22	−0.139	5.14	⋯	4.8
Pd	2.47	−0.089	5.56	⋯	3.2
Ti	2.13	−0.417	4.73	⋯	−3.7

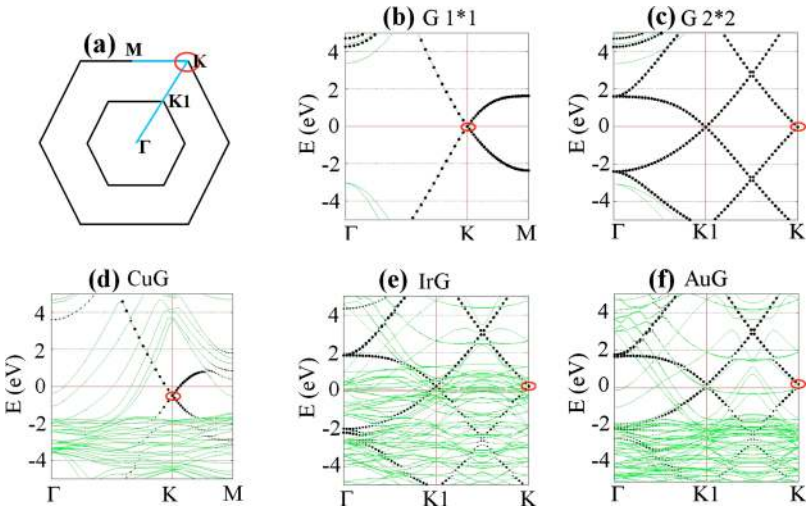

FIG. 2. (Color online) (a) Shows the BZ of 1×1 and 2×2 unit cells. The inner hexagon is the first BZ of graphene's 2×2 unit cell with half size of the outer hexagon which is the first BZ of graphene's 1×1 unit cell. (b) and (c) show the electronic band structures of the graphene for 1×1 and 2×2 unit cell calculations with the black dots representing the intensity of π-orbital components. (d)–(f) show the electronic structures of three interface models with the Dirac points indicated by ellipses.

sizes of supercells and graphene carbon atoms fixed. The ionic relaxation is stopped when the total energy change between two subsequent relaxation steps is smaller than 1 meV. Monkhorst–Pack k-point sampling grids of 33×33 and 20×20 are used for the 1×1 and 2×2 2D Brillouin zone (BZ). $50\times50\times600$ and $98\times98\times600$ fast Fourier transform (FFT) meshes in 1×1 and 2×2 unit cell's real spaces are adopted for accurate charge analysis. Spin-polarized calculations are used exclusively for two common ferromagnetic metals of Ni and Co. The EEF effect is modeled by two parallel sheets (with an equivalent amount of opposite charges on each sheet) inserted in the vacuum region. The maximum electrostatic potential energy in the vacuum region of the freestanding metal is chosen as the common vacuum level when comparing energy-levels of isolated metal, isolated graphene and the metal-graphene complex.

III. RESULTS AND DISCUSSIONS

We have carried out first-principles calculations to investigate graphene's adsorption on twelve different metal substrates which have been commonly used in making metal/graphene contacts. Based on the simulation results (Table I), the investigated metal substrates can be classified into two distinctive categories according to adsorption energies, adsorption distances and orbital hybridization. For weak interaction (physisorption) interfaces between graphene and metals (formed for seven metal substrates consisting of Al, Ag, Cu, Cd, Ir, Pt, and Au), adsorption energies are around 0.03–0.05 eV per carbon atom, with equilibrium interfacial distances >3.0 Å. Charge transfer happens at these interfaces and leads to doping of graphene. For strong interaction (chemisorption) interfaces between graphene and metals (formed for five metal substrates consisting of Ni, Co, Ru, Pd, and Ti), adsorption energies are larger at around 0.09 $\sim$0.4 eV per carbon atom, with smaller equilibrium interfacial distances <2.5 Å. Orbital hybridization is substantial at these interfaces and alters graphene's intrinsic π-band structures near Fermi level. These basic findings are consistent with experimental observations in the recent experimental works by Vogel *et al.*[26] and Wallace *et al.*[27] In Vogel *et al.*'s fabricated devices, Ni, Ti/Au and Pd are found to be easily deposited on graphene as electrodes to form stable contacts. However, Pt and Au are found to be very easily detached from graphene and hard to stick coherently on graphene. Wallace *et al.*'s XPS data show that there is carbide bonding formation at Ti–Graphene interface, but no carbide bonding is observed at Pt-Graphene interface.

Our further investigation shows that at physisorption interfaces, the Pauli-exclusion principle takes effect between the metal atom's outermost *s*-electrons and graphene's π-electrons and significantly shifts down graphene's energy levels relative to metal's electronic states. Nevertheless, the complex's common Fermi level is determined by metal substrates. These two factors result in a "discrepancy" between graphene's charge neutrality level and the complex's common Fermi level, and subsequently drive interface charges to transfer leading to graphene's doping. On the other hand, at chemisorption interfaces, orbital hybridization occurs since small interfacial distances cause a wave function overlap between metal's *d*-electrons and graphene's π-electrons. Hybridization effect is most pronounced in the energy range close to metal's *d*-band electronic structure. Graphene's original π-states dispersion is shifted away from the hybridization region due to orbital repulsion, leaving behind a π-band "gap" with large amount of hybridized π-states. Motivated by these results, we have applied an external electric field to induce a relative shift between metal *d*-band and graphene π-band which provides not only a supporting argument to verify the energy-levels shift in graphene, but also a viable engineering approach to artificially control metal–graphene interactions.

A. Physisorption interfaces

Band structures of Cu–, Ir–, and Au–Graphene (CuG, IrG, and AuG) as representatives of physisorption interfaces are shown in Fig. 2. Although K1 in the first BZ of 2×2 unit cell is identical to K in the first BZ of 1×1 unit cell (see Fig. 2), for the 2×2 graphene unit cell models [Figs. 1(c) and 1(f)], we still extend k-point sampling to K for a direct comparison with 1×1 unit cell's band structure. Due to the folded BZ in the 2×2 models, we obtained an additional pair of energy levels (Dirac point at K1) besides the pair of

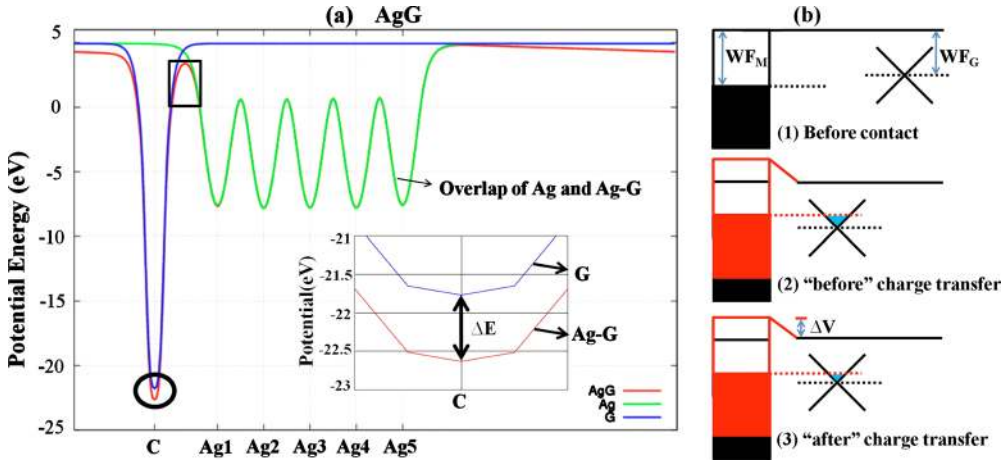

FIG. 3. (Color online) (a) Potential lineups of Ag-G complex, Ag and G, the black rectangular box indicates the tunneling barrier. Fermi level is set at E =0. (b) Three separate steps of M–G interface interactions as graphene approaches the metal surface (*n*-doped graphene presented). "before" and "after" charge transfer are two artificially separate steps for physical illustration of the role of transferred charge rather than sequential behaviors in realistic interface interactions.

levels crossing (Dirac point) at K point as expected, but we will focus on the pair of levels crossing at K point since K1 is equivalent to K. At physisorption interfaces, graphene's intrinsic band structure with linear band crossing at K (Dirac point) is preserved, but the Dirac point is shifted corresponding to doping as indicated by the ellipses in Fig. 2.

The results in Table I and Fig. 2 clearly show that even those metals (e.g., Cu with WF=5.35 eV) with intrinsic WF larger than that of graphene (WF=4.77 eV) can *n*-dope graphene. Both previous theoretical[18] and experimental[20] works have observed this peculiar doping effect. Interface dipoles play a critical role resulting in a potential step at M–G interface, which modifies the Schottky-Mott model with an additional term ΔV. Nevertheless, it is worthwhile to point out clearly that ΔV is a net result of the Pauli-exclusion interaction and a self-compensation effect from the transferred charge, where the charge transfer is a secondary effect rather than a primary effect. For some interfaces such as Ir–G, the large WF difference ($\Delta\phi$=5.82 eV−4.77 eV =1.05 eV) between Ir and Graphene is balanced without obvious charge transfer ($\Delta q \approx 0$ in Bader charge analysis,[38] and experimental observation[23] shows graphene is slightly *p*-doped by Ir substrate). In fact, graphene can be *n*-doped only when graphene's charge neutrality level is relatively shifted down below the metal's Fermi level. Even though it has been suggested that the change of the metal's WF by graphene's covering[18] is responsible for the graphene doping, the detailed mechanisms of WF changes are not yet clearly understood. Our study shows that the "primary effect" is the relative shift down of graphene's energy-levels due to Pauli-exclusion interaction with metal.

In order to examine the relative shift down of graphene's energy-levels, we have aligned a uniform reference vacuum energy in in-plane averaged potential lineups of G, Ag, and Ag–G complex as shown in Fig. 3. The difference of graphene's potential before (G line) and after (AgG line) contacting with a metal clearly shows that graphene's energy-levels shift down [ΔE in Fig. 3(a) inset] due to the interaction with metal substrate. The almost exact overlap of a clean metal's (Ag line) and the M-side of the M–G interface (AgG line) potentials provides a direct evidence that complex's Fermi level is determined by the metal slab. For most cases, graphene's charge neutrality level will not be exactly shifted to align with the metals' Fermi levels since the Pauli repulsion interaction will result in distinctive modification of the WFs of metal and graphene as shown in Fig. 3(b) middle panel. This diagram shows that the metal WF has a larger decrease than that of graphene, and this is due to the large electron density at the metal surface which is pushed into the metal by the graphene π-electrons. In contrast, graphene's π-electrons may not change much since any redistribution of π-electrons requires a hybridization with *s*-orbital which is energetically unfavorable. After the significant shift up of metal's chemical potential, there is a new discrepancy between the complex's common Fermi level and graphene's charge neutrality level. This "discrepancy" drives the charge transfer at the interface from metal to graphene or vice versa depending on the relative shift of WFs. When charge transfer happens, a self-charge electrostatic-field is generated and further shifts graphene's energy-levels up (*n*-doped graphene) or down (*p*-doped graphene), reducing this "discrepancy" [shown in Fig. 3(b) bottom panel]. The reduction in the "discrepancy" is a self-compensation mechanism from transferred charge. Note that there is a tunneling barrier at the interface [indicated by a rectangular box in Fig. 3(a)] which separates the transferred charges in real space. We have estimated the tunneling probability at Ag–G interface (assuming a square potential barrier with barrier height 4 eV and barrier width 1.8 Å) and found an approximate transmission probability of 20% which is considerable. Therefore, at physisorption interfaces, tunneling barriers are not expected to reduce carrier injection greatly at the metal-graphene contacts. This finding is consistent with experimental findings of Vogel[26] in which contact resistances between graphene and different metal contacts (including both physisorption and chemisorption metals) do not show much changes.

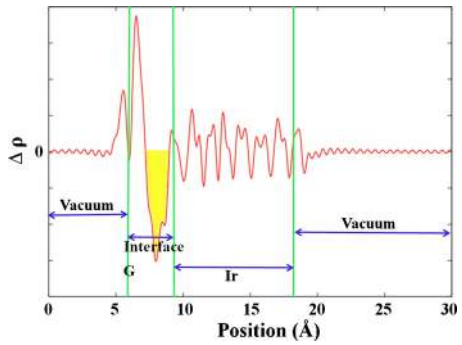

FIG. 4. (Color online) Charge difference ($\Delta\rho=\rho_{complex}-\rho_{Metal}-\rho_{Graphene}$) plot along vertical axis. Graphene is at z=6 Å and Ir metal slab is at 9.5 Å<z<19 Å. The interface at around 7.0 Å<z<8.5 Å shows a charge depletion.

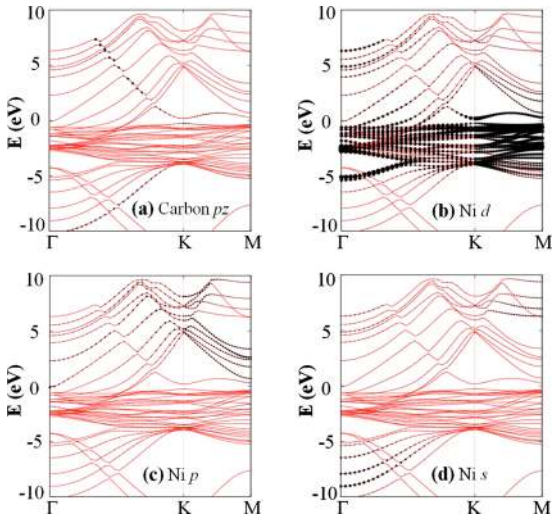

FIG. 5. (Color online) Spin-up state electronic band structure of Ni–G complex. Black dots show the intensities of (a) carbon *pz*-orbital, (b) Ni *d*-orbital, (c) Ni *p*-orbital, and (d) Ni *s*-orbital components. (a) Graphene π-band shows a gap opening with bonding states below the Ni *d*-band and antibonding states above the *d*-band. (b) Ni *d*-band is relatively flat and strongly hybridized with C π-band. (c) Ni *p*-orbitals are sparse. (d) Ni *s*-orbitals are forming a broad band from −10 to 10 eV in the figure.

At the Ir–G interface, considerable energy-levels shift of ~0.8 eV [0.8 eV≈5.82 eV−4.77 eV−0.23 eV (ΔE_F in Table I)] is calculated even without obvious charge transfer between metal and graphene. This effect is quite similar to what has been observed in closed-shell noble gas Xe atoms adsorbed on metal surfaces.[39] The stability of the closed shell atom does not allow a charge transfer or chemical bonding at the adsorption, but the Pauli-exclusion principle plays a dominant role in redistributing electron densities within the Xe atom and on the metal surface. It may not be easy to directly apply Bagus' method[39] to graphene's adsorption on metal surfaces because graphene has sp^2 bonding and partially occupied π-states rather than closed shell orbitals in Xe atom. Nevertheless, the analysis of charge density difference plot (Fig. 4) shows that typical Pauli-exclusion-induced charge redistribution appears at the Ir–G interface. The charge density difference shows that the electrons are pushed away from the interface (indicated by negative $\Delta\rho$ zone at around 7.0 Å<z<8.5 Å) into the metal and graphene subsurface (indicated by a positive $\Delta\rho$ near the interface for both graphene and metal slab). In this paper, the terminology "charge transfer" is used to represent the net charge transfer from one atom to another atom, and the terminology "charge redistribution" to represent charge density change within the same atom (e.g., asymmetric peaks of $\Delta\rho$ in graphene in Fig. 4). Figure 4 shows a clear pictorial illustration that the Ir atom has a reduced charge density at the interface which supports the existence of the Pauli-exclusion interaction since only the charge transfer mechanism would have increased the charge density around Ir atoms because of graphene's slight *p*-doping. This charge density difference plot provides a strong evidence that Pauli-exclusion interaction is the primary effect in determining the relative shift of the WFs. When metal surface atoms approach graphene, the metal's outermost *s*-electrons with a large radial electron density distribution will overlap with graphene's π-electrons, and the Pauli-exclusion interaction will be correspondingly induced. It is this repulsive interaction that pushes the electron distributions back into both metal's and graphene's subsurface away from the interface. Graphene is a surfacelike material without bulk materials' reservoir of a large amount of electrons. Consequently, the Pauli-exclusion interaction cannot change the graphene's electron density distribution significantly so that the WF decrease is negligible, as indicated in Fig. 3(b). In contrast, the metal surface electron density can be redistributed by rehybridizing the surface electronic orbitals leading to a larger WF change. Dipoles are formed during the process of the Pauli-exclusion interaction in Fig. 3(b) middle panel, and then weakly compensated by transferred charge in Fig. 3(b) bottom panel. Moreover, we have explicitly shown that the metal–graphene interaction is neither an electrostatic interaction nor chemical interaction based on the following two observations. (1) The electrostatic potential energy originating from the metal side decays to a negligible value (smaller than 0.1 eV) at the graphene side; (2) There is no significant electron wave function overlap (representing chemical bonding) between metal and graphene, which is consistent with the band structures (Fig. 2) and also indicated by a sizable tunneling barrier at the interface (Fig. 3). The Pauli-exclusion interaction strength has a sizable variation among different metal-graphene interfaces because different metals have different densities of *s*-states corresponding to different overlap strengths with graphene π-states. The lower electron density of the *s*-band has a weaker Pauli-exclusion strength because of the reduced wave function overlap.

B. Chemisorption interfaces

For a graphene chemisorbed on Ni, Co, Ru, Pd, or Ti substrates, the band structure shows a strong change from graphene's intrinsic π-band electronic structure including the Dirac point. Figure 5 shows the spin-up state electronic structure of graphene on a Ni substrate, and the carbon *pz* (C*pz*), Ni *d*, *p*, and *s* orbital contributions are projected as black dots on the band structure with the dot size representing the intensity of the orbital components. Figure 6 shows the C*pz* orbital projections of the graphene on Pd, Ti, and Ni

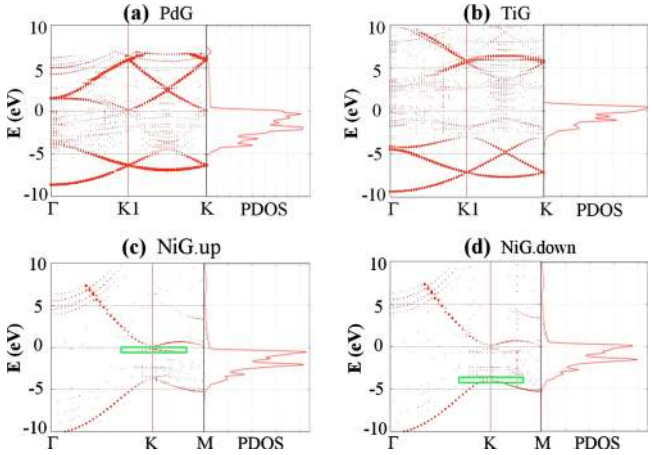

FIG. 6. (Color online) Left panel of each figure shows the intensity of C*pz* states on the M–G complex electronic band structures. Right panel shows the corresponding *d*-band density of states in clean metal. (a) Pd–G complex shows a π-band gap between −4 and 0 eV which corresponds to the Pd *d*-band DOS. (b) Ti–G complex shows a π-band gap between −3 and 3 eV which is a bit wider than the Ti *d*-band DOS. (c) and (d) are spin "up" and "down" states of the Ni–G complex which show that the C*pz* states are strongly influenced by the magnetic property of the Ni substrate.

[Fig. 6(c) corresponding to Fig. 5(a)]. The C*pz* states share the following common properties. (1) At the metal *d*-states distribution energy region [from ~−4 eV to ~0 eV for Ni as shown in Figs. 6(c) and 6(d)], the C*pz* states are strongly hybridized with metal *d*-states as indicated by the C*pz* orbital contributions. (2) The π-band energy levels are pushed down (up) below (above) hybridization region. (3) Excluding the "gap" filled with hybridized states, C*pz* electronic states above and below the hybridization region recover graphene's intrinsic π-band shape with bonding and anti-bonding states separated by a band gap. There is a considerable density of "gap states" within the hybridization region which renders the graphene metallic rather than "semimetallic" at the interface. The small equilibrium interfacial distance and large amount of gap states eliminate the tunneling barrier which exists at physisorption interfaces.

For the chemisorption interfaces, orbital hybridization dominates graphene's band gap opening with additional contributions from Pauli-exclusion interactions. As the interfacial distance decreases to an equilibrium chemisorption distance, the Pauli-exclusion interaction becomes stronger and the energy-levels of graphene shift down further relative to that of metals. However, the π-electron wave function also begins to overlap with the metal *d*-electron wave function and an orbital hybridization interaction occurs. The hybridization interaction strongly modifies graphene's intrinsic π-states dispersion (e.g., the Dirac point), and hybridized states exist in a certain energy range of metal *d*-states (Figs. 5 and 6). These hybridized states push unoccupied π-states to higher energy through repulsive energy level interactions. As a result, hybridization is mainly accompanied by two electronic structure properties consisting of a strong mixture between metal *d*- and graphene π-states and π-band gap opening. The resulting electronic structure of chemisorbed graphene is a π-band gap opening with randomly distributed gap states. In order to examine the details of graphene electronic structure changes, only projected C*pz* components are plotted in Fig. 6.

In Fig. 6, we show both π-band structures for graphene on Pd, Ti, and Ni substrates and the density of states (DOS) of *d*-orbitals of clean metals side by side. The magnetic property of Ni substrate induces different electronic structures for spin-up and spin-down states for both Ni substrate and graphene as shown in Figs. 6(c) and 6(d). Hybridization (indicated by distributed π-orbital contributions in the π-band gap) occurs over the metal *d*-states distribution energy region, except for a mismatch at Ti-G case [Fig. 6(b)]. The mismatch for the Ti-G case is consistent with its larger binding energy than other interfaces as listed in Table I. Note that the *d*-band DOS in Fig. 6 are calculated from clean metals rather than M–G complexes since we aim to predict graphene's π-band gap energy range based on metal's intrinsic bulk properties (e.g., *d*-band energy range in a clean metal). We have shown that the graphene π-band gap energy range at the Ti–G interface, although wider above the *d*-band edge of clean bulk Ti, is consistent with *d*-orbitals energy range of interface Ti atoms. So, the mismatch indicates that strong interaction of Ti–G interface expands the *d*-orbital's DOS of interface Ti atoms compared to that of bulk Ti atoms. Therefore, the hybridization region (π-band gap) is exactly consistent with the clean metal's *d*-states distribution energy region at the M–G chemisorption interface of intermediate interface interaction strengths (e.g., Ni–G or Pd–G). The better preservation of the top of the π-valence-band near the Fermi level for spin up states than spin down states at Ni–G interface [rectangular boxes in Figs. 6(c) and 6(d)] is consistent with the lower energy distribution of Ni's spin-up *d*-electrons than Ni's spin-down *d*-electrons. Comparison between Figs. 6(c) and 6(d) indicates that the hybridization is spin-dependent for ferromagnetic metals-graphene interactions.

C. EEF effect

In the analysis of interface electronic structures, the graphene doping is shown to be determined by the intrinsic interactions between the graphene π-bands and the metal surface electrons. There is a recent experimental report that the graphene WF can be controlled within 4.5–4.8 eV by an electric field effect.[40] Motivated by this experimental finding, we have examined the effect of EEF on the metal–graphene interface electronic structure. Since the graphene WF was modulated by the back gate without forming metal-graphene interfaces, it is not clear how the back gate would change the graphene WF when a metal contact is formed on top of the graphene layer. To investigate the interface electronic structure change induced by the back gate voltage, we have introduced an EEF simulating the back gate potential in the metal-graphene interface model. The electric field strength was controlled by the double layer charge dipole introduced in the 18 Å vacuum region as discussed in the Methodology section. It is expected that EEF can further shift graphene's energy-levels in Fig. 3(b), (1) modulating doping densities and even doping types in physisorption interfaces and (2)

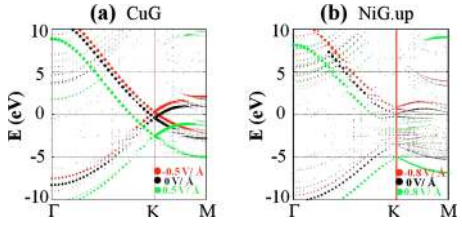

FIG. 7. (Color online) Graphene π-bands (Cpz components) of Cu–G (representing physisorption interface) are plotted for three EEFs −0.5, 0, and 0.5 eV/Å. Graphene π-bands of spin-up Cpz components of Ni–G (representing chemisorption interface) are plotted for three EEFs −0.8, 0, and 0.8 eV/Å.

modulating graphene's hybridized electronic structure and interaction strength in chemisorption interfaces.

Figure 7 shows the electronic structures of representative physisorption (Cu–G) and chemisorption (Ni–G) interfaces with EEF applied. Applying a vertical EEF with strength increasing from a negative value to a positive value, graphene's doping densities are modulated gradually and even doping types can be reversed in the physisorption interface. Since the Fermi level is pinned by the metal substrate in the physisorption complex, the EEF can shift graphene's energy-levels up and down relative to the Fermi level (E =0 in Fig. 7). Therefore, by adjusting EEF strength one can modulate the relative positions between graphene's charge neutrality level and complex's common Fermi level at the metal-graphene interface leading to an accurate control of graphene's doping types and densities. In the chemisorption complex, hybridization takes place in the metal's *d*-band energy distribution range, and the variable EEF strength can adjust different parts of graphene's band structure to hybridize with metal's *d*-bands. Due to distinctive density of states at different parts of graphene's band structure, the EEF can tune different amount of states into hybridization, and thus the hybridization strength can be sizable. The physical mechanism behind this practical EEF application is that graphene's WF can be effectively tuned by EEF. For graphene-based device applications, local back-gate voltages below the metal-graphene contacts can be used to realize accurate localized doping.

IV. SUMMARY

In conclusion, systematic calculations of graphene adsorbed on 12 different metal substrates show that all these interfaces can be classified into two categories of physisorption and chemisorption interactions. At physisorption interfaces, there is little wave function overlap and Pauli-exclusion repulsion changes electronic states of metal's *s*-electrons and graphene's π-electrons leading to a relative shift down of graphene's energy-levels below metal surface electronic states. However, the complex's Fermi level is determined by the metal substrate, and charge transfer takes place as a secondary effect, driven by the discrepancy between graphene's charge neutrality level and complex's common Fermi level. At chemisorption interfaces, due to a large wave function overlap between metal's *d*-electrons and graphene's π-electrons, graphene's intrinsic π-band structure is significantly changed. Both the Pauli-exclusion repulsion effect on energy-level shift and hybridized states' repulsive interactions result in graphene's π-band gap opening with randomly distributed gap states. The gap states are formed by the hybridized states, and contribute to push the graphene's unoccupied energy-states to higher energy and the corresponding gap opening. Finally, the effect of EEF (simulating a back gate bias voltage) has shown a possibility of an efficient control of the interface electronic structure of metal-graphene complexes. Applied EEF on graphene can shift grpahene's energy-levels and modulate doping or hybridization. These findings can help facilitate possible ways to control doping and interface interactions in realistic devices.

ACKNOWLEDGMENTS

This work is funded by Southwest Academy of Nanotechnology (SWAN). Calculations are done on Texas Advanced Computer Center (TACC). We thank the SWAN team members for insightful discussions during weekly graphene meeting at UT Dallas.

[1]K. S. Novoselov, A. K. Geim, S. V. Morozov, D. Jiang, Y. Zhang, S. V. Dubonos, I. V. Grigorieva, and A. A. Firsov, Science **306**, 666 (2004).
[2]K. S. Novoselov, A. K. Geim, S. V. Morozov, D. Jiang, M. I. Katsnelson, I. V. Grigorieva, S. V. Dubonos, and A. A. Firsov, Nature (London) **438**, 197 (2005).
[3]Y. Zhang, Y.-W. Tan, H. L. Stormer, and P. Kim, Nature (London) **438**, 201 (2005).
[4]V. P. Gusynin and S. G. Sharapov, Phys. Rev. Lett. **95**, 146801 (2005).
[5]X. Wang, Y. Ouyang, X. Li, H. Wang, J. Guo, and H. Dai, Phys. Rev. Lett. **100**, 206803 (2008).
[6]H. W. Ch. Postma, Nano Lett. **10**, 420 (2010).
[7]C. A. Merchant, K. Healy, M. Wanunu, V. Ray, N. Peterman, J. Bartel, M. D. Fischbein, K. Venta, Z. Luo, A. T. C. Johnson, and M. Drndić, Nano Lett. **10**, 2915 (2010).
[8]G. F. Schneider, S. W. Kowalczyk, V. E. Calado, G. Pandraud, H. W. Zandbergen, L. M. K. Vandersypen, and C. Dekker, Nano Lett. **10**, 3163 (2010).
[9]S. Garaj, W. Hubbard, A. Reina, J. Kong, D. Branton, and J. A. Golovchenko, Nature (London) **467**, 190 (2010).
[10]S. Y. Zhou, G.-H. Gweon, A. V. Fedorov, P. N. First, W. A. De Heer, D.-H. Lee, F. Guinea, A. H. Castro Neto, and A. Lanzara, Nature Mater. **6**, 770 (2007).
[11]E. Rollings, G.-H. Gweon, S. Y. Zhou, B. S. Mun, J. L. McChesney, B. S. Hussain, A. V. Fedorov, P. N. First, W. A. de Heer, and A. Lanzara, J. Phys. Chem. Solids **67**, 2172 (2006).
[12]M. Ishigami, J. H. Chen, W. G. Cullen, M. S. Fuhrer, and E. D. Williams, Nano Lett. **7**, 1643 (2007).
[13]G. Bertoni, L. Calmels, A. Altibelli, and V. Serin, Phys. Rev. B **71**, 075402 (2005).
[14]P. W. Sutter, J.-I. Flege, and E. A. Sutter, Nature Mater. **7**, 406 (2008).
[15]S. Marchini, S. Günther, and J. Wintterlin, Phys. Rev. B **76**, 075429 (2007).
[16]A. T. N'Diaye, S. Bleikamp, P. J. Feibelman, and T. Michely, Phys. Rev. Lett. **97**, 215501 (2006).
[17]B. Uchoa, C.-Y. Lin, and A. H. C. Neto, Phys. Rev. B **77**, 035420 (2008).
[18]G. Giovannetti, P. A. Khomyakov, G. Brocks, V. M. Karpan, J. van den Brink, and P. J. Kelly, Phys. Rev. Lett. **101**, 026803 (2008).
[19]B. Huard, N. Stander, J. A. Sulpizio, and D. Goldhaber-Gordon, Phys. Rev. B **78**, 121402(R) (2008).
[20]K. Pi, K. M. McCreary, W. Bao, W. Han, Y. F. Chiang, Y. Li, S.-W. Tsai, C. N. Lau, and R. K. Kawakami, Phys. Rev. B **80**, 075406 (2009).
[21]K. T. Chan, J. B. Neaton, and M. L. Cohen, Phys. Rev. B **77**, 235430 (2008).
[22]D. Eom, D. Prezzi, K. T. Rim, H. Zhou, M. Lefenfeld, S. Xiao, C. Nuckolls, M. S. Hybertsen, T. F. Heinz, and G. W. Flynn, Nano Lett. **9**, 2844 (2009).
[23]I. Pletikosić, M. Kralj, P. Pervan, P. Brako, J. Coraux, A. T. N'Diaye, C. Busse, and T. Michely, Phys. Rev. Lett. **102**, 056808 (2009).
[24]S. Barraza-Lopez, M. Vanevic, M. Kindermann, and M. Y. Chou, Phys.

Rev. Lett. **104**, 076807 (2010).
[25]X. Li, W. Cai, J. An, S. Kim, J. Nah, D. Yang, R. Piner, A. Velamakanni, I. Jung, E. Tutuc, S. K. Banerjee, L. Colombo, and R. S. Ruoff, Science **324**, 1312 (2009).
[26]A. Venugopal, L. Colombo, and E. M. Vogel, Appl. Phys. Lett. **96**, 013512 (2010).
[27]A. Pirkle, R. M. Wallace, and L. Colombo, Appl. Phys. Lett. **95**, 133106 (2009).
[28]Q. J. Wang and J. G. Che, Phys. Rev. Lett. **103**, 066802 (2009).
[29]M. Vanin, J. J. Mortensen, A. K. Kelkkanen, J. M. Garcia-Lastra, K. S. Thygesen, and K. W. Jacobsen, Phys. Rev. B **81**, 081408(R) (2010).
[30]A. Varykhalov, J. Sánchez-Barriga, A. M. Shikin, C. Biswas, E. Vescovo, A. Rybkin, D. Marchenko, and O. Rader, Phys. Rev. Lett. **101**, 157601 (2008).
[31]A. Grüneis and D. V. Vyalikh, Phys. Rev. B **77**, 193401 (2008).
[32]Y. Gamo, A. Nagashima, M. Wakabayashi, M. Terai, and C. Oshima, Surf. Sci. **374**, 61 (1997).
[33]S. Gowtham, R. H. Scheicher, R. Ahuja, R. Pandey, and S. P. Karna, Phys. Rev. B **76**, 033401 (2007).
[34]G. Kresse and J. Furthmüller, Comput. Mater. Sci. **6**, 15 (1996).
[35]P. E. Blöchl, Phys. Rev. B **50**, 17953 (1994).
[36]C. Kittel, *Introduction to Solid State Physics*, 7th ed. (Wiley, New York, 1996).
[37]J. Neugebauer and M. Scheffler, Phys. Rev. B **46**, 16067 (1992).
[38]G. Henkelman, A. Arnaldsson, and H. Jónsson, Comput. Mater. Sci. **36**, 354 (2006).
[39]P. S. Bagus, V. Staemmler, and C. Wöll, Phys. Rev. Lett. **89**, 096104 (2002).
[40]Y.-J. Yu, Y. Zhao, S. Ryu, L. E. Brus, K. S. Kim, and P. Kim, Nano Lett. **9**, 3430 (2009).